


Article

Study of the $\text{La}_{1-x}\text{Sr}_x\text{MnO}_3$ Cathode Film Prepared by a Low Power Plasma Spray Method with Liquid Solution Precursor for a Solid Oxide Fuel Cell

Chih-Hao Lee ^{1,*} , Bing-Syun Yeh ¹ and Tsun-Neng Yang ²
¹ Department of Engineering and System Science, National Tsing Hua University, Hsinchu 30013, Taiwan

² Institute of Nuclear Energy Research, Lungtan, Taoyuan 32546, Taiwan

* Correspondence: chlee@mx.nthu.edu.tw; Tel.: +886-0912-090-253

Abstract: A perovskite $\text{La}_{1-x}\text{Sr}_x\text{MnO}_3$ cathode thin film for an oxygen ion conducting solid oxide fuel cell was prepared using a low power (8.8 kW) liquid solution plasma spray method. Usually, a 30–50 kW Ar plasma torch with temperature higher than all the melting points of solid precursors is essential to synthesis oxides thin film. However, using the liquid precursors as the feeding materials, the required power can be reduced and save a lot of thermal budget. The precursors are water solutions of lanthanum nitrate hexahydrate, manganese(II) nitrate tetrahydrate, and strontium nitrate. The atomic percentage of La in the plasma sprayed $\text{La}_{1-x}\text{Sr}_x\text{MnO}_3$ cathode film is lower than that of La in the feeding precursor into the torch, which is due to the low boiling temperature of $\text{La}(\text{NO}_3)_3$ precursor. The oxygen stoichiometry of $\text{La}_{1-x}\text{Sr}_x\text{MnO}_{3-\delta}$ deduced from the valence state of Mn measured by X-ray absorption spectroscopy shows an oxygen deficit structure. The measured low resistivity of 0.07–0.09 Ωcm at room temperature for this $\text{La}_{1-x}\text{Sr}_x\text{MnO}_{3-\delta}$ is essential for oxygen ion transport in the cathode thin film of a solid-state fuel cell.

Keywords: plasma spray coating; $\text{La}_{1-x}\text{Sr}_x\text{MnO}_3$ thin film; solid state fuel cell; liquid precursors



Citation: Lee, C.-H.; Yeh, B.-S.; Yang, T.-N. Study of the $\text{La}_{1-x}\text{Sr}_x\text{MnO}_3$ Cathode Film Prepared by a Low Power Plasma Spray Method with Liquid Solution Precursor for a Solid Oxide Fuel Cell. *Crystals* **2022**, *12*, 1633. <https://doi.org/10.3390/cryst12111633>

Academic Editor: Dmitry Medvedev

Received: 30 September 2022

Accepted: 9 November 2022

Published: 14 November 2022

Publisher's Note: MDPI stays neutral with regard to jurisdictional claims in published maps and institutional affiliations.



Copyright: © 2022 by the authors. Licensee MDPI, Basel, Switzerland. This article is an open access article distributed under the terms and conditions of the Creative Commons Attribution (CC BY) license (<https://creativecommons.org/licenses/by/4.0/>).

1. Introduction

The perovskite $\text{La}_{1-x}\text{Sr}_x\text{MnO}_{3-\delta}$ (LSM) thin film is a common material for the cathode of an oxygen ion conducting solid oxide fuel cell (SOFC) operated at high temperature (800–1000 °C), which can be used as a high efficiency small power station for a local community. Usually, the SOFCs use hydrogen as the fuel without carbon emission. The efficiency can be better than 60%, which is much higher than that of a traditional coal power plants (32–40%) and nuclear power plants (25–33%). In an oxygen ion conducting SOFC, the anode side collects electrons and converts the hydrogen into water vapor, while the cathode side converts the oxygen molecules from the air into oxygen ions and emits electrons. The oxygen ions generated from cathode then transports through the ceramic electrolyte to the anode to react with hydrogen atoms [1–3]. Among the variety of cathode materials studied for SOFC applications, perovskite materials are the most researched cathodes for SOFC so far [4–6]. Manganese based perovskite, such as $\text{La}_{1-x}\text{Sr}_x\text{MnO}_3$, shows high electrical conductivity and matched thermal expansion coefficient with conventional YSZ (Yttria-Stabilized-Zirconia) electrolyte is the most popular cathode material in the high temperature SOFC. A number of preparation methods, such as solid-state reaction, sol-gel technique, hydrothermal synthesis, spray drying, co-precipitation, and combustion, have been used for perovskite synthesis [7–9]. After the perovskite powder was obtained, usually, screen printing and sintering were used to prepare the cathode film on the electrolyte layer of SOFC. Plasma spray is an alternative method to prepare the thin films of SOFC. The plasma spray consists of many advantages, such as high density, good adhesion, and ease of mixing composite materials. Furthermore, by changing the concentration ratio of feeding precursors, a graded layer on both sides of electrolyte can be prepared in order to match

the gradual change in oxygen or fuel concentration near the electrolyte. A careful control of the melting, quenching, and consolidation processes of the ceramic materials on the substrate can be conducted by varying the deposition parameters, such as feeding rate, the torch to substrate distance, and substrate temperature [10]. In the past, the plasma spray method was applied on fabricating the electrolyte, anode, and cathode electrode films [11–22]. However, most of the plasma sprayers need a high power in order to melt all the feeding tiny solid powder precursors. For example, Kang et al. [13] used 35 kW of plasma spray technique, Orlando et al. [14] used 37 kW, White et al. [15] used a torch more than 50 kW, and Nie et al. used 31 kW [16] to coat the LSM materials. To reduce the cost of plasma spray and save the thermal budget, continuously feeding the precursor with liquid solution instead of feeding with nano-particle solid precursors, a lower power plasma spray can be achieved. This Solution Precursor Plasma Spray (SPPS) method is getting popular in coating electrolytes and electrodes of SOFC [17–22]. Using liquid phase SPPS is more flexible to fabricate a graded chemical composition of cathode or anode on the electrolyte of an SOFC. This graded electrode can be easily spray coated with SPPS by changing the ratio of different kinds of the liquid precursors as function of time. In addition, it can be easier to prepare doped materials by adding new components into the liquid precursors.

In this work, we use the SPPS method to coat the cathode LSM thin film of SOFC with a low power (8.8 kW) plasma spray torch. The resulting sprayed LSM films were tested and material properties of the thin films were studied. Contrary to the solid precursor feeding with a high-power plasma spray machine, we found that the chemical composition of LSM thin film is deviated from the composition of precursors. The result is a drawback for the low power plasma spray system with liquid solution precursors, but it can be compensated easily by feeding different compositions at beginning. In the following, we will illustrate this low power SPPS method for the fabrication of LSM thin film of an SOFC.

2. Experimental

Figure 1 is a schematic of a plasma spray machine built by Institute of Nuclear Energy Research, Taiwan. The main chamber (20 cm long) of the sprayer is a plasma torch. The distance between the torch and the substrate is 15 cm. The plasma torch is ignited under 10 L/min of Ar and then changed to N₂ as the operation gas. The typical operation condition for N₂ is 4 kg/cm² and 15 L/min monitoring by a rotameter (F311, Lorric Inc., New Taipei City, Taiwan). The two-phase flow feeding nozzle consists of two input channels, a liquid precursor input and an N₂ input as a carrier gas. The typical feeding rate of liquid precursor is 0.5–1 mL/min, which is controlled by a peristaltic pump (BT100-2J, Longer Precision Pump Co., Hebei, China) with a load peristaltic pump head (YZ1515W, Longer Precision Pump Co., Hebei, China). The typical operation current is 40 A and the operation voltage is 220 V. The torch temperature was monitored using a pyrometer (Endurance Series, E1MH, Fluke Inc., Everett, WA, USA) before the deposition. The precursors are water solution of lanthanum nitrate hexahydrate (Sigma-Aldrich, 99.9%), manganese (II) nitrate tetrahydrate (Sigma-Aldrich, 98%), and strontium nitrate (Riedel-de Haen, 99%), each one with a typical 1 M in concentration. This solution is injected directly into the torch. Figure 2 shows a result of Computation Fluid Dynamics (CFD) simulation calculation [23] with temperature distribution in the arc of this plasma spray machine. At this 8.8 kW power level, the maximum temperature in the torch is higher than 3400 °C. The solution of precursor was injected in the torch at a position 1.2 cm from the beginning of the torch where the temperature is around 2600 °C. This temperature is higher than the required temperature of 800 °C to form LSM according to the ternary phase diagram [24] of the La₂O₃, Mn₂O₃ and SrO system. The injected solution was vaporized and dried quickly. At the same time, all the nitrates were melted and formed the LSM particles at downstream. Under this condition, the deposition rate of the cathode film was about 1.5 µm/min on the YSZ substrate. Typically, 100 µm thin films were prepared for material characterizations. The resulting LSM thin films were then characterized by XRD (X-ray

diffraction, 5020 diffractometer, Huber Diffraktionstechnik GmbH, Rimsting, Germany) to determine the structures, XRF (X-ray Fluorescence, XR-100CR, Amptek Inc., Bedford, OH, USA) and ICP-AES (Inductively Coupled Plasma- Atomic Emission Spectroscopy, Avio 220 Max, PerkinElmer Inc., Waltham, MA, USA) to determine the composition; SEM (Scanning Electron Microscopy, JSM-6700F, JEOL Ltd., Tokyo, Japan) operated at 20 keV in secondary electron imaging mode to understand the morphology and XANES (X-ray Absorption Near Edge Structure) on the Mn K-edge was used to determine the oxidation states of Mn in these SPPS thin films. The XRD and XANES experiments were carried out at TLS17B and TLS17C beamlines at National Synchrotron Radiation Research Center, Taiwan. These beamlines are installed with a Si(111) double crystal monochromator resulting in an energy resolution of 0.2 eV [25]. For the resistivity measurement, a four-probe resistance measurement was also performed to obtain the sheet resistance of the deposition film.

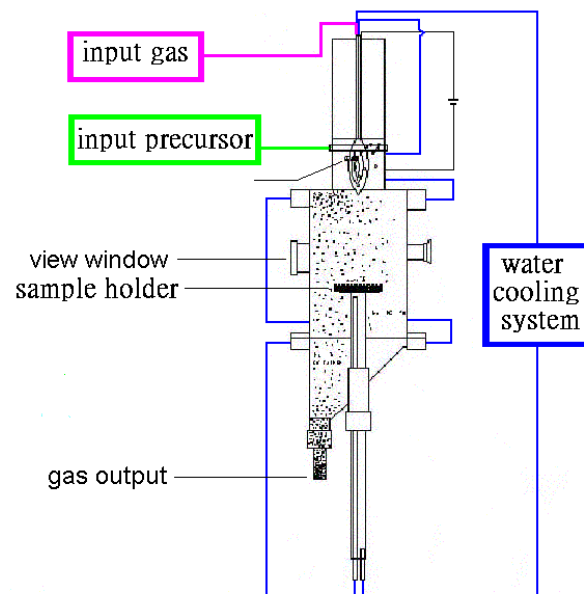


Figure 1. Schematic plot of the plasma spray apparatus. Input carrier gas system in purple; input liquid precursors system in green; the water cooling system in blue.

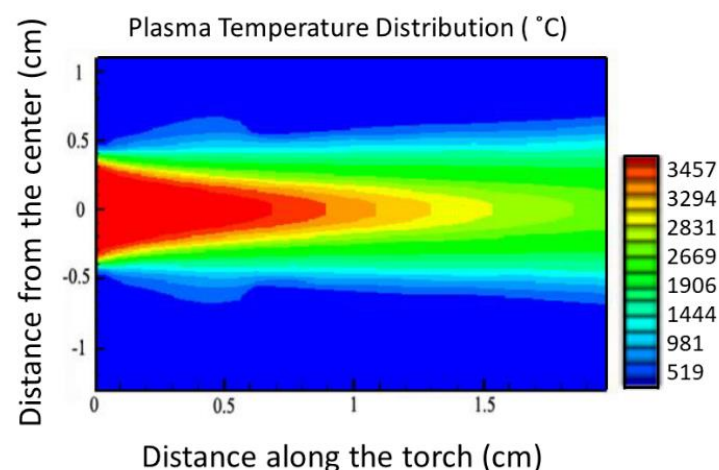


Figure 2. The temperature distribution of the plasma torch by a CFD simulation.

3. Results and Discussion

The structure of deposited LSM thin films with the atomic percentage of La/Sr from 1:2 to 3:1 in precursor solutions were checked by the XRD as shown in Figure 3. The lattice parameters can be fitted by a tetragonal perovskite phase using TEROR program [26].

However, orthorhombic LSM phase can also be fitted quite well also. Coexistence of tetragonal and orthorhombic cannot be ruled out. The lattice parameters of (100) as functions of Sr compositions are shown in Figure 4, together with a few published lattice parameters of LSM [27–32]. The lattice parameters (100) of our samples match quite well with those previous results prepared by different process methods. Since the ion radius of Sr^{2+} (0.144 nm with coordination number of 12) [33] is larger than the ion radius of La^{3+} (0.136 nm with coordination number of 12) [33], as the atomic percentage of Sr increases, the lattice parameter (100) shrinks. The diffraction peaks are broadened by the small particle size of around 5–20 nm determined by the Scherrer's formula. By measuring the diffraction peak width of [200], [112] and [220], the coherent lengths of the nano-particles of LSM showed twice more elongated around [110] direction, which indicates the nanoparticle has a rod-like shape. The particle size of LSM can be tuned by the concentration of the liquid precursors. The higher concentration of precursor usually results in a higher chance of coagulation into larger particles. For example, for 1 M solution, the particle size is usually 60% larger than that of using 0.1 M of precursor solution. This small particle size is suitable for the electrode materials of a SOFC due to its higher surface to volume ratio which provides more triple phase boundaries for the oxygen molecules to convert into ions and transfer into the electrolyte with electron transport via electrodes. The XRD also shows coexistence of many impurity phases and broaden peaks. The drawback of the plasma spray system is the difficulty to control the composition within a short time in torch, due to its non-equilibrium nature. The structure of the thin films depending on the locations and temperatures inside the torch. The small impurity peaks are not easy to be identified due to the complex composition of three precursor system. The major impurity phase is La_2O_3 resulting in a loss of La atomic percentage in the final LSM films. The broaden diffraction peaks might also indicate a mixed phase of tetragonal and orthorhombic phases [27,31]. However, the major phase is still identified as tetragonal phase. Nevertheless, these different phases also create high porosity in the plasma sprayed film, which is beneficial for O_2 to penetrate into the cathode film of SOFC to improve the rate of oxygen reduction reaction.

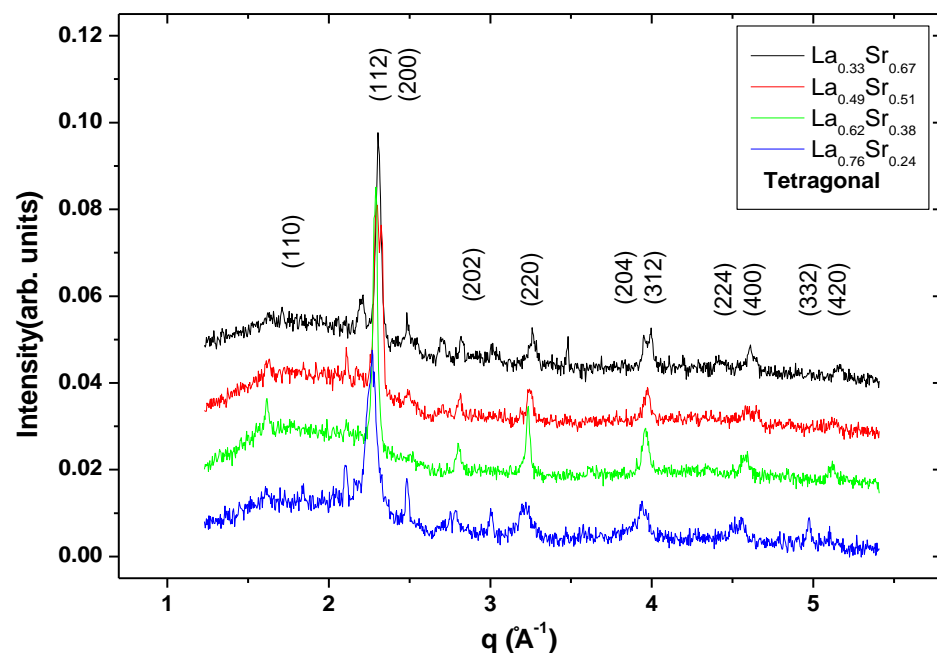


Figure 3. The XRD pattern of plasma spray deposited $\text{La}_{1-x}\text{Sr}_x\text{MnO}_{3-\delta}$ films. The $q = 4\pi\sin\theta/\lambda$ where θ is the incident angle of X-ray and λ is 0.124 nm, the wavelength of X-ray.

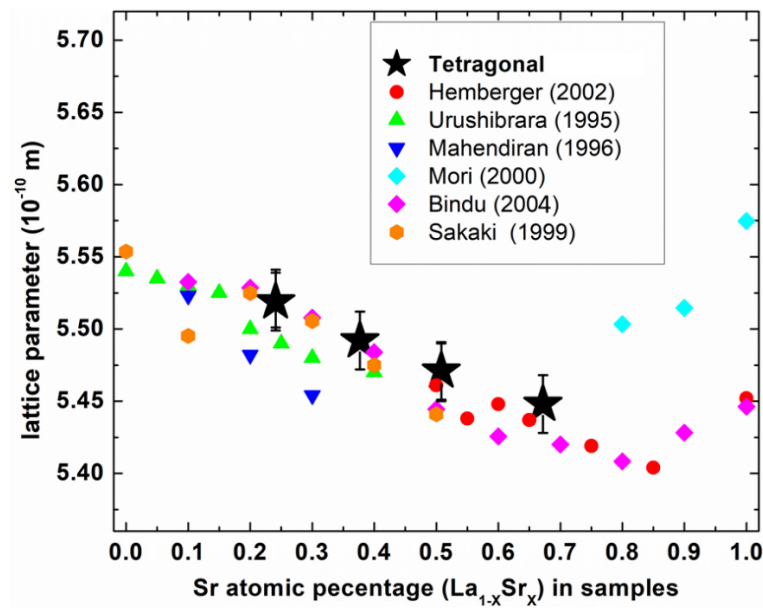


Figure 4. The lattice parameters (100) in $\text{La}_{1-x}\text{Sr}_x\text{MnO}_3$ unit cells as functions of Sr atomic percentages together with a few published lattice parameters [27–32].

Figure 5 shows the SEM picture of plasma sprayed LaMnO_3 , SrMnO_3 , and $\text{La}_{0.5}\text{Sr}_{0.5}\text{MnO}_3$. We can see that the small nano-particles are aggregated into a cluster of a few μm . Porosity can be found on the surface of the deposited film. By using the Image-J program [34], for the plasma sprayed LaMnO_3 , SrMnO_3 the porosity is around 20% and for $\text{La}_{0.5}\text{Sr}_{0.5}\text{MnO}_3$, 33% of porosity is obtained. The morphology of $\text{La}_{0.5}\text{Sr}_{0.5}\text{MnO}_3$ thin film is not as uniform as that of LaMnO_3 and SrMnO_3 , because it needs three elements, La, Sr, and Mn, to form a doped LSM, which is more complex than a two-precursor system. The particle size distribution of the $\text{La}_{0.5}\text{Sr}_{0.5}\text{MnO}_3$ film is also more dispersive than that of two precursor system.

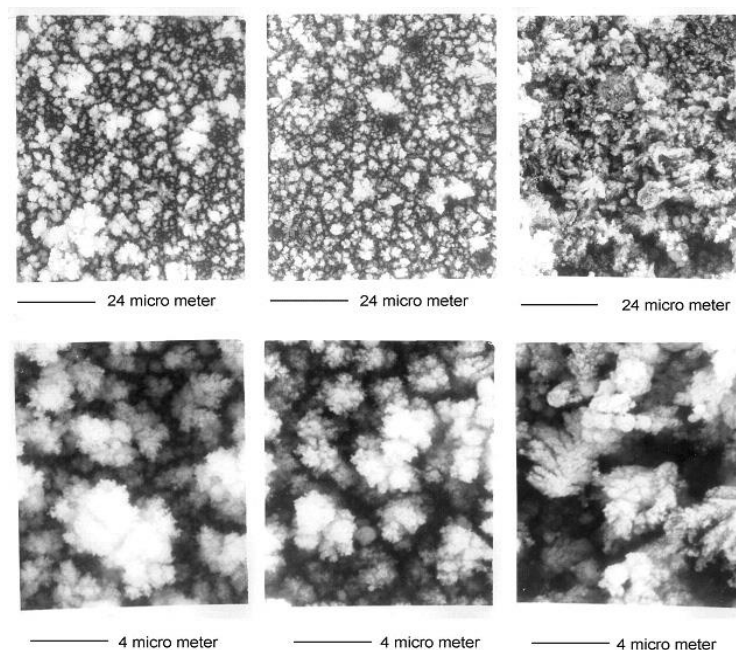


Figure 5. SEM pictures for LaMnO_3 (left), SrMnO_3 (middle), and $\text{La}_{0.5}\text{Sr}_{0.5}\text{MnO}_3$ (right). The upper figures are magnified by 1000 times and the lower ones are 6000 times.

In order to study the calcination and reaction of the mixture of precursor solution inside the plasma torch system, a series of different atomic ratios of La/Sr precursors were

tested. We found the atomic ratios of La/Sr in the LSM thin films on the substrates are different from those ratios added in the precursor solution at beginning. Figure 6 shows the deviation of La/(La + Sr) ratio in the LSM samples determined by XRF and ICP-AES. The atomic percentage of La in the plasma sprayed $\text{La}_{1-x}\text{Sr}_x\text{MnO}_3$ cathode film is lower than the atomic percentage of La feeding precursors into the torch. This might be due to the evaporation pressure of each nitrate solution being different. When the mixed nitrate solution was injected into the torch, the water vaporized first. Since the boiling point of $\text{La}(\text{NO}_3)_3$ is 399 K, which is much lower than that of $\text{Sr}(\text{NO}_3)_2$ (918 K), most of $\text{La}(\text{NO}_3)_3$ molecules were vaporized or decomposed first, while $\text{Sr}(\text{NO}_3)_2$ molecules travelled a longer distance before completely evaporated or decomposed; a lower composition of La/Sr ratio was found along the forward direction of the torch. We also scratched some of the residual LSM powder from the chamber wall at a distance of 0 cm to 30 cm from the torch, the La/Sr ratio of the sample decreases as the distance increases (see Figure 7). This result again shows a loss of $\text{La}(\text{NO}_3)_3$ vapor along the forward direction of the plasma torch. To compensate the loss of La atoms on LSM films, an additional amount of $\text{La}(\text{NO}_3)_3$ molecules should be added in the liquid precursor at beginning.

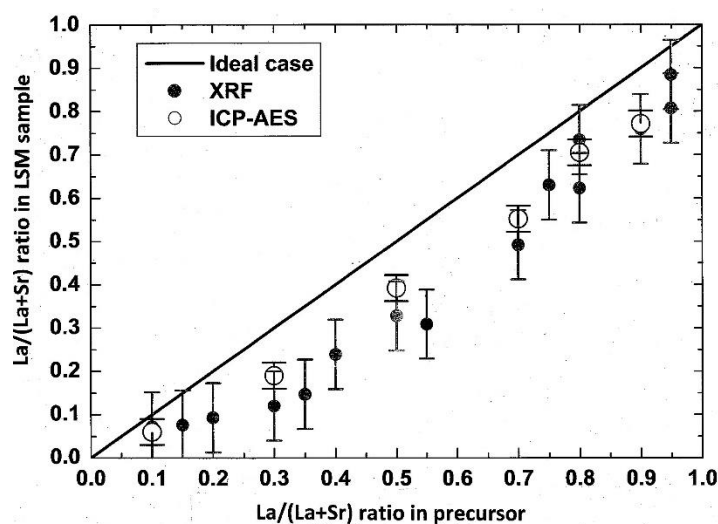


Figure 6. The deviation of La/(La + Sr) composition ratios in the plasma sprayed LSM films determined by XRF and ICP-AES to compare with that in the initial precursor solutions. The straight line is the ratio of ideal case if the composition is not changed.

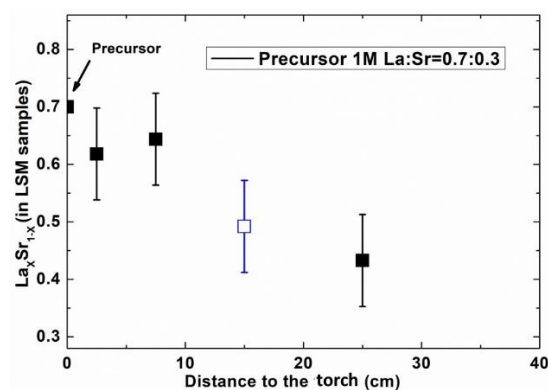


Figure 7. The La/(La + Sr) composition ratio of LSM samples as a function of the distance from the torch (close squares). The open square (blue) is the La/(La + Sr) composition ratio on the substrate which 15 cm from the torch. The La/Sr ratio in the liquid precursor is 70/30 at beginning.

The catalyst function of LSM is to have oxygen reduction reaction on the triple phase boundary and migrate the oxygen ions to the oxygen ion conducting electrolyte [35].

When the LSM operated at high temperature, it usually possesses an oxygen deficit state, especially when the oxygen pressure is not high [35,36]. In order to study whether the oxygen vacancies were formed in the plasma sprayed LSM films, XANES study on the Mn K-edge was performed (shown in Figure 8). The valence state of Mn in the sample can be obtained from the K-edge shift of the XANES spectra using the linear interpolation among the K-edges of MnO, Mn₂O₃, and MnO₂ standard powder samples [37]. In this work, the valence states of Mn of all samples on the substrates at different locations are within +3 and +4. Depending on the composition ratio of La/Sr, and the valence state of Mn, the deviation of oxygen stoichiometry in the LSM can be determined. For example, in the case of 2.5 M precursor solution with La/Sr = 3/1, which corresponds to the atomic percentage of Sr of $x = 0.5 \pm 0.05$ of plasma sprayed film on the substrate, the Mn K-edge was found at 6.5395 keV. This K-edges shift corresponds to a Mn valence state of +3.4 and gives rise to an oxygen deficit of $\delta = 0.05 \pm 0.03$. This oxygen deficit thin film enhances the catalyst effect on oxygen reduction reaction [35] and is also beneficial to the oxygen ion transport in the cathode film.

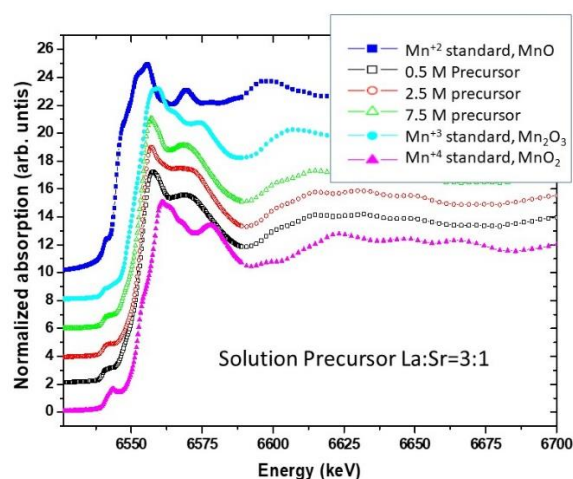


Figure 8. A typical XANES spectra at Mn K edges of La_{1-x}Sr_xMnO_{3-δ} samples.

The resistivity of these LSM ($x = 0.4$ – 0.9) samples measured using four probe measurements is within 0.07–0.09 Ωcm at room temperature. The resistivity of our plasma sprayed films is close to the work previously reported [8,38,39] and two times smaller than the results of Prabhakaran et al. [40], but ten times larger than the values reported by Ohtani et al. [41]. The low resistance of these plasma sprayed films typically satisfy the resistivity value of commercial cathode materials (0.01–0.1 Ωcm at room temperature), which also shows that the cathode material prepared by this low power plasma spray is feasible for fabricating the cathode film of an SOFC.

4. Conclusions

In summary, a low-power plasma spray method to prepare an LSM cathode film for a SOFC was studied for the first time. To save the thermal budget, using the liquid phase precursors as the feeding materials is essential to decrease the required power in the preparation of LSM cathode films. The structure of the LSM films was characterized by XRD, SEM, XRF, ICP-AES, four probe resistance measurement, and XANES and showed that the material properties of SPPS LSM film is close to the bulk perovskite LSM structure with nano-size grains of around 5–20 nm, which is suitable for SOFC applications. However, a deficit of atomic percentage of La in the SPPS films were found in comparison to that of initial feeding solution precursors. In order to control the right composition, more concentrated La(NO₃)₃ solution in the precursors should be added to compensate the loss of La in the torch. The liquid precursor plasma spray system can be operated at much

lower power in comparison to those high-power plasma spray machines using the micro-size solid precursors.

Author Contributions: Conceptualization, T.-N.Y. and C.-H.L.; resources, T.-N.Y.; experimental validation and data analysis, B.-S.Y.; writing—original draft preparation, C.-H.L. and B.-S.Y.; writing—review and editing, C.-H.L. All authors have read and agreed to the published version of the manuscript.

Funding: This project is supported by National Science and Technology Council, R.O.C., under the contract no of NSC93-2623-7-007-010-NU.

Data Availability Statement: Not applicable.

Acknowledgments: We are grateful to have the beam time provided by National Synchrotron Radiation Research Centre, Taiwan. The plasma spray machine is assembled and supported by Institute of Nuclear Energy Research, Taiwan.

Conflicts of Interest: The authors declare no conflict of interest.

References

1. Kuterbekov, K.A.; Nikonov, A.V.; Bekmyrza, K.Z.; Pavzderin, N.B.; Kabyshev, A.M.; Kubenova, M.M.; Kabdrakhimova, G.D.; Aidarbekov, N. Classification of Solid Oxide Fuel Cells. *Nanomaterials* **2022**, *12*, 1059. [\[CrossRef\]](#) [\[PubMed\]](#)
2. Singh, M.; Zappa, D.; Comini, E. Solid oxide fuel cell: Decade of progress, future perspectives and challenges. *Int. J. Hydrogen Energy* **2021**, *46*, 27643–27674. [\[CrossRef\]](#)
3. Dwivedi, S. Solid oxide fuel cell: Materials for anode, cathode and electrolyte. *Int. J. Hydrogen Energy* **2020**, *45*, 23988–24013. [\[CrossRef\]](#)
4. Ahmad, M.Z.; Ahmad, S.H.; Chen, R.S.; Ismail, A.F.; Hazan, R.; Baharuddin, N.A. Review on recent advancement in cathode material for lower and intermediate temperature solid oxide fuel cells application. *Int. J. Hydrogen Energy* **2021**, *47*, 1103–1120. [\[CrossRef\]](#)
5. Ndubuisi, A.; Abouali, S.; Singh, K.; Thangadurai, V. Recent advances, practical challenges, and perspectives of intermediate temperature solid oxide fuel cell cathodes. *J. Mater. Chem. A* **2021**, *10*, 2196–2227. [\[CrossRef\]](#)
6. Jun, A.; Kim, J.; Shin, J.; Kim, G. Perovskite as a Cathode Material: A Review of its Role in Solid-Oxide Fuel Cell Technology. *ChemElectroChem* **2016**, *3*, 511–530. [\[CrossRef\]](#)
7. da Conceição, L.; Ribeiro, N.F.; Furtado JG, M.; Souza, M.M. Effect of propellant on the combustion synthesized Sr-doped LaMnO₃ powders. *Ceram. Int.* **2009**, *35*, 1683–1687. [\[CrossRef\]](#)
8. Kaur, P.; Singh, K. Review of perovskite-structure related cathode materials for solid oxide fuel cells. *Ceram. Int.* **2020**, *46*, 5521–5535. [\[CrossRef\]](#)
9. Harrison, C.M.; Slater, P.R.; Steinberger-Wilckens, R. A review of Solid Oxide Fuel Cell cathode materials with respect to their resistance to the effects of chromium poisoning. *Solid State Ion.* **2020**, *354*, 115410. [\[CrossRef\]](#)
10. Herman, H.; Sampath, S.; McCune, R. Thermal Spray: Current Status and Future Trends. *MRS Bull.* **2000**, *25*, 17–25. [\[CrossRef\]](#)
11. Hwang, C.; Yu, C.-H. Formation of nanostructured YSZ/Ni anode with pore channels by plasma spraying. *Surf. Coat. Technol.* **2007**, *201*, 5954–5959. [\[CrossRef\]](#)
12. Hwang, C.; Tsai, C.H.; Lo, C.H.; Sun, C.H. Plasma sprayed metal supported YSZ/Ni-LSGM-LSCF ITSOFC with nanostructured anode. *J. Power Sources* **2008**, *180*, 132–142. [\[CrossRef\]](#)
13. Kang, H.K.; Taylor, P.R.; Lee, J.H. Characterization of La_{0.8}Sr_{0.2}MnO₃ produced by a reactive DC thermal plasma spray system. *Plasma Chem. Plasma Process.* **2003**, *23*, 223–232. [\[CrossRef\]](#)
14. Orlando, M.; Cunha, A.; Freitas, J.; Orlando, C.; Bud'Ko, S.; Giordanengo, B.; Sato, I.; Martinez, L.; Baggio-Saitovitch, E. Structure and magnetotransport properties in plasma-sprayed La_{0.78}Sr_{0.22}MnO₃ thick film. *J. Magn. Magn. Mater.* **2002**, *246*, 10–15. [\[CrossRef\]](#)
15. White, B.; Keßler, O.; Rose, L. Air plasma spray processing and electrochemical characterization of SOFC composite cathodes. *J. Power Sources* **2008**, *178*, 334–343. [\[CrossRef\]](#)
16. Nie, H.; Huang, W.; Wen, T.-L.; Tu, H.; Zhan, Z. LSM cathodes for SOFC prepared by plasma spraying. *J. Mater. Sci. Lett.* **2002**, *21*, 1951–1953. [\[CrossRef\]](#)
17. Bhatia, T.; Ozturk, A.; Xie, L.; Jordan, E.H.; Cetegen, B.M.; Gell, M.; Ma, X.; Padture, N. Mechanisms of ceramic coating deposition in solution-precursor plasma spray. *J. Mater. Res.* **2002**, *17*, 2363–2372. [\[CrossRef\]](#)
18. Chen, D.; Jordan, E.H.; Gell, M. Effect of solution concentration on splat formation and coating microstructure using the solution precursor plasma spray process. *Surf. Coat. Technol.* **2008**, *202*, 2132–2138. [\[CrossRef\]](#)
19. Kuo, Y.-L.; Kencana, S.D.; Su, Y.-M.; Huang, H.-T. Tailoring the O₂ reduction activity on hydrangea-like La_{0.5}Sr_{0.5}MnO₃ cathode film fabricated via atmospheric pressure plasma jet process. *Ceram. Int.* **2018**, *44*, 7349–7356. [\[CrossRef\]](#)
20. Metcalfe, C.; Lay-Grindler, E.; Kesler, O. Characterization of Ni-YSZ anodes for solid oxide fuel cells fabricated by solution precursor plasma spraying with axial feedstock injection. *J. Power Sources* **2014**, *247*, 831–839. [\[CrossRef\]](#)

21. Prakash, B.S.; Kumar, S.S.; Aruna, S.T. Microstructure and performance of LSM/YSZ based solid oxide fuel cell cathodes fabricated from solution combustion co-synthesized powders and by solution precursor plasma spraying. *Surf. Coat. Technol.* **2017**, *310*, 25–32. [CrossRef]
22. Khan, M.; Hu, N.; Zhenhua, L.; Wang, Y.; Yi, Z. Influence of solution-precursor plasma spray (SPPS) processing parameters on the mechanical and thermodynamic properties of 8 YSZ. *Ceram. Int.* **2018**, *44*, 7794–7798. [CrossRef]
23. Trelles, J.P. Finite Element Methods for Arc Discharge Simulation. *Plasma Process. Polym.* **2017**, *14*, 1600092. [CrossRef]
24. Thermfact and GTT-Technologies. Available online: <http://www.FactSage.com> (accessed on 31 May 2019).
25. Tsang, K.L.; Lee, C.H.; Jean, Y.C.; Dann, T.E.; Chen, J.R.; D’Amico, K.L.; Oversluisen, T. The Wiggler X-ray Beamlines at SRRC. *Rev. Sci. Instrum.* **1995**, *66*, 1812–1814. [CrossRef]
26. Werner, P.E.; Eriksson, L.; Westdahl, M. TREOR, a semi-exhaustive trial-and-error powder indexing program for all symmetries. *J. Appl. Crystallogr.* **1985**, *18*, 367–370. [CrossRef]
27. Hemberger, J.; Krimmel, A.; Kurz, T.; von Nidda, H.A.K.; Ivanov, V.Y.; Mukhin, A.A.; Balbashov, A.M.; Loidl, A. Structural, magnetic, and electrical properties of single-crystalline $\text{La}_{1-x}\text{Sr}_x\text{MnO}_3$ ($0.4 < x < 0.85$). *Phys. Rev. B* **2001**, *66*, 094410.
28. Urushibrara, A.; Moritomo, Y.; Arima, T.; Asamitsu, A.; Kido, G.; Tokura, Y. Insulator-metal transition and giant magnetoresistance in $\text{La}_{1-x}\text{Sr}_x\text{MnO}_3$. *Phys. Rev. B* **1995**, *51*, 14103–14109. [CrossRef]
29. Mahendiran, R.; Tiwary, S.K.; Raychaudhuri, A.K.; Ramankrishnan, T.V.; Mahesh, R.; Rangavittal, N.; Rao, C.N.R. Structure, electron-transport properties, and giant magnetoresistance of hole-doped systems. *Phys. Rev. B* **1996**, *53*, 3348–3358. [CrossRef]
30. Mori, T.; Inoue, K.; Kamegashira, N. Phase behavior in the system $\text{La}_x\text{Sr}_{1-x}\text{MnO}_{(5+x)/2}$ ($x = 0.8\text{--}1.0$) with trivalent state of manganese ion. *J. Alloys Compd.* **2000**, *308*, 87–93. [CrossRef]
31. Bindu, R. Structural studies of $\text{La}_{1-x}\text{Sr}_x\text{MnO}_{3+\delta}$ ($x = 0.1\text{--}1.0$). *Eur. Phys. J. B Condens. Matter Complex Syst.* **2004**, *37*, 321–327. [CrossRef]
32. Sakaki, Y.; Takeda, Y.; Kato, A.; Imanishi, N.; Yamamoto, O.; Hattori, M.; Esaki, Y. $\text{Ln}_{1-x}\text{Sr}_x\text{MnO}_3$ (Ln = Pr, Nd, Sm and Gd) as the cathode material for solid oxide fuel cells. *Solid State Ion.* **1999**, *118*, 187–194. [CrossRef]
33. Shannon, R.D. Revised Effective Ionic Radii and Systematic Studies of Interatomic Distances in Halides and Chalcogenides. *Acta Crystallogr.* **1976**, *32*, 751–767. [CrossRef]
34. National Institute of Health. Available online: <https://imagej.nih.gov/ij/> (accessed on 20 May 2019).
35. Li, Y.; Gemmen, R.; Liu, X. Oxygen reduction and transportation mechanisms in solid oxide fuel cell cathodes. *J. Power Sources* **2010**, *195*, 3345–3358. [CrossRef]
36. Mizusaki, J.; Yonemura, Y.; Kamata, H.; Ohyama, K.; Mori, N.; Takai, H.; Tagawa, H.; Dokiya, M.; Naraya, K.; Sasamoto, T. Electronic conductivity, Seebeck coefficient, defect and electronic structure of nonstoichiometric $\text{La}_{1-x}\text{Sr}_x\text{MnO}_3$. *Solid State Ion.* **2000**, *132*, 167–180. [CrossRef]
37. Liu, R.S.; Jang, L.Y.; Chen, J.M.; Wu, J.B.; Liu, R.G.; Lin, J.G.; Huang, C.Y. X-ray absorption near edge structure studies of colossal magnetoresistance ferromagnet $(\text{La}_{1.4}\text{Sr}_{1.6})\text{Mn}_2\text{O}_7$. *Solid State Commun.* **1998**, *105*, 605–608. [CrossRef]
38. Abdelmoula, N.; Guidara, K.; Cheikh-Rouhou, A.; Dhahri, E.; Joubert, J.C. Effects of the oxygen nonstoichiometry on the physical properties of $\text{La}_{0.7}\text{Sr}_{0.3}\text{MnO}_3$ manganites. *J. Solid State Chem.* **2000**, *151*, 139–144. [CrossRef]
39. Shimura, T.; Hayashi, T.; Inaguma, Y.; Itoh, M. Magnetic and electrical properties of $\text{La}_y\text{A}_x\text{Mn}_w\text{O}_3$ (A = Na, K, Rb, and Sr) with Perovskite-Type Structure. *J. Solid State Chem.* **1996**, *124*, 250–263. [CrossRef]
40. Prabhakaran, D.; Coldea, A.I.; Boothroyd, A.T.; Blundell, S.J. Growth of large $\text{La}_{1-x}\text{Sr}_x\text{MnO}_3$ single crystals under argon pressure by the floating-zone technique. *J. Cryst. Growth* **2002**, *237*, 806–809. [CrossRef]
41. Ohtani, T.; Kuroda, K.; Matsugami, K.; Katoh, D. Electrical resistivity and thermopower of $(\text{La}_{1-x}\text{Sr}_x)\text{MnO}_3$ and $(\text{La}_{1-x}\text{Sr}_x)\text{CoO}_3$ at elevated temperatures. *J. Eur. Ceram. Soc.* **2000**, *20*, 2721–2726. [CrossRef]